Chiang Mai J. Sci. 2018; 45(2) : 1122-1128
http://epg.science.cmu.ac.th/ejournal/
Contributed Paper

Comparison of Sizes, Morphologies and Optical Properties of NiO Nanostructures Synthesized Using Acetate and Nitrate Anions from Nickel Salts via Hydrothermal Method

Pranwadee Kaewmuang [a], Watcharapong Pudkon [a], Anurak Prasatkhetragarn [b], Piyarat Nimmanpipug [a], Sila Kittiwachana [a], Sulawan Kaowphong* [a]

[a] Department of Chemistry, Faculty of Science, Chiang Mai University, Chiang Mai 50200, Thailand.

[b] Department of Materials Science, School of Science, University of Phayao, Phayao 56000, Thailand.

* Author for correspondence; e-mail: sulawank@gmail.com

Received: 12 October 2016
Accepted: 29 December 2016

ABSTRACT

Porous NiO nanocrystals were synthesized using a hydrothermal method in mediums of different anions from nickel salts, acetate (CH_3COO^-) and nitrate (NO_3^-),followed by calcination at 500 °C. Firstly, β-$Ni(OH)_2$ powders with a hexagonal structure were formed. Using acetate and nitrate anions, the obtained β-$Ni(OH)_2$ powders were composed of thin nanosheets (0.8-2.1 μm in length), and a splinter-like structure self-assembled with longer nanosheets (9.8-24.2 μm), respectively. The difference in the interaction ability between the anions and the β-$Ni(OH)_2$ surfaces, affecting the growth behavior of the crystals, was examined using the density functional theory (DFT) method. After calcination, the β-$Ni(OH)_2$ turned into porous NiO with a cubic structure but their morphologies were unchanged. The porous NiO with longer nanosheets possessing higher crystallinity and larger surface area provided better UV-Vis absorption ability.

Keywords: NiO, semiconductor, nanocrystalline material, X-ray technique, electron microscopy, optical property

1. INTRODUCTION

Nickel oxide (NiO) is an interesting p-type semiconductor with a wide band gap (3.6-4.0 eV). Excellent optoelectrical properties make NiO nanostructures suitable for various applications, such as electrochemistry [1], magnetic materials [2], dye-sensitized photocathodes [3], gas sensors [4] and catalysts [5]. The properties of semiconductor materials depend not only on their structure and composition, but also on their size and morphology. Therefore, a number of attempts have been made to synthesize materials with controllable size and morphology in order to obtain the desired properties. Different morphologies of NiO nanostructures, such as flower-like [4], nanosheets [5], honeycomb-like [6], nanoplates [7], microspheres [8], and

octahedral [9], have been synthesized by various methods [4-9]. Among these methods, the hydrothermal method provides fine particles with high crystallinity and purity at a relatively low temperature due to generated pressure. Typically, nanomaterials with the desired characteristics can be synthesized by controlling some synthesis parameters such as temperature, time, pH, solvent, and additives. In addition, under the same conditions, different starting reagents can also tailor the shapes and sizes of the synthesized nanomaterials.

This research investigated the effects of two different anions from nickel salts - acetate (CH_3COO^-) and nitrate (NO_3^-) - on the size, morphology and optical property of NiO nanostructures synthesized by the hydrothermal method. The density functional theory (DFT) method was used to evaluate the interaction ability between the anions and crystal surfaces, affecting the crystal growth behavior.

2. MATERIALS AND METHODS

2.1 Preparation

Nickel acetate ($Ni(CH_3COO)_2 \cdot 4H_2O$, 99.0%) or nickel nitrate ($Ni(NO_3)_2 \cdot 6H_2O$, 99.0%) of 5 mmol was dissolved in 80 mL of deionized water. After constant stirring for 30 mins, the solution was transferred into a Teflon-lined stainless steel autoclave with a capacity of 160 mL. The autoclave was sealed, heated at 200 °C for 24 hrs, and naturally cooled to room temperature. A light green powder was collected, washed with deionized water and then dried at 80 °C overnight. Finally, the collected powder was further calcined at 500 °C for 3 hrs with heating rate of 2 °C/min, resulting in a black powder. The powders, synthesized using nickel acetate and nickel nitrate, were named A and N, respectively. The NiO powders, obtained by calcining A and N powders, were named A500 and N500, respectively.

2.2 Characterization

The synthesized powders were characterized by X-ray diffractometer (XRD, Rigaku Miniflex II) with CuK_α radiation. Vibrational modes of the powders were investigated by Fourier transform infrared spectroscopy (FTIR, Bruker TENSOR27). Particle size and morphology of the powders were determined using a field emission scanning electron microscope (FESEM, JEOL JSM-6335F), operating at 15 kV of accelerating voltage, and a transmission electron microscope (TEM, JEOL JEM-2010), operating at 200 kV. Specific surface areas were measured by the Brunauer-Emmett-Teller method (BET, Autosorb 1 MP, Quantachrome). Chemical compositions were analysed by energy dispersive X-ray (EDX) spectroscopy with an accelerating voltage of 15 kV. UV-Vis absorption spectra were recorded by UV-Vis spectroscopy (Lamda25 PerkinElmer, U.S.A.)

3. RESULTS AND DISCUSSION

Figures1(a) and 1(b) show the XRD patterns of the powders synthesized using different nickel salts before and after calcination, respectively. In Figure1(a), the diffraction peak positions of the N and A samples are well consistent with those of the hexagonal β-$Ni(OH)_2$structure (JCPDS database no.14-0117). The intensity of the (001) peak is significantly strengthened compared to that of the JCPDS pattern. This suggests that the β-$Ni(OH)_2$ crystals have a preferential crystal growth along the *c*-axis[10]. The ratio of the peak intensity of the (001) and the (101) of the A and N patterns is clearly different. The diffraction peaks of the (001) of the N pattern is stronger than that of the A pattern, indicating the

existence of an unusual nanostructure and more preferential crystal growth along the *c*-axis in the N sample [11]. A detailed microstructure information of the synthesized products is further confirmed by SEM and TEM images. After calcination, the diffraction peaks corresponding to cubic NiO (JCPDS database no. 78-0429) are observed as shown in Figure1(b). No other characteristic peaks of β-Ni(OH)$_2$ are detected, indicating that β-Ni(OH)$_2$ completely transformed to NiO. The intensities of the diffraction peaks of the N500 NiO powder are relatively higher than that of A500 NiO powder, suggesting the improved crystallization of the NiO particles.

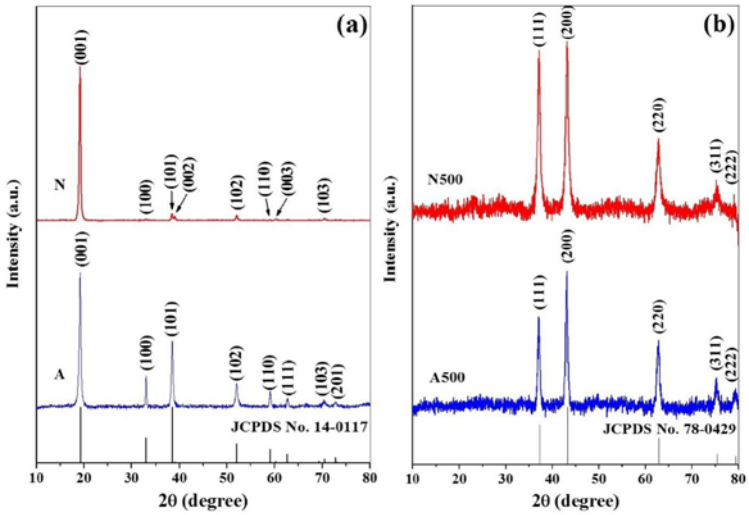

Figure 1. XRD patterns of the powders synthesized using different nickel salts(a) before and (b) after calcination.

FTIR spectra of the powders synthesized using different nickel salts are shown in Figure 2. The FTIR spectra of the A and N powders show a narrow band at 3644 cm^{-1} which is attributed to the O-H stretching vibration of the hydroxyl groups of β-Ni(OH)$_2$ [12, 13]. The weak peaks at 1380 cm^{-1} and 1040 cm^{-1} are assigned to carbonate ions [14], which could be attributed to the dissolution of CO_2 from air. A weak band at 460 cm^{-1} and broad band at 518 cm^{-1} are assigned to Ni-O stretching and in-plane Ni-O-H bending vibrations [13], respectively. The FTIR spectra of the A500 and N500 NiO powders show bands at 426 cm^{-1} and 558 cm^{-1} which are attributed to the Ni-O stretching vibration of NiO_6 octahedrons in the cubic NiO structure [15]. Notably, the broad peak from 3490 cm^{-1} to 3000 cm^{-1} and a weak band at 1610 cm^{-1} are attributed to adsorbed water on the sample surfaces [13].

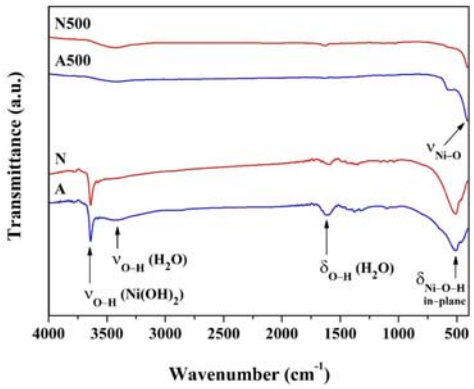

Figure 2. FTIR spectra of the β-Ni(OH)$_2$ and NiO powders synthesized using different nickel salts.

The FESEM image of the A powder (Figure 3(a)) composes of nanosheets with a thickness of 50-100 nm and edge size of 0.8-2.1 µm. While, FESEM image of the N powder (Figure 3(b)) composes of a splinter-like structure self-assembled with long nanosheets in the range of 9.8-24.2 µm. Previous studies [7, 15] have reported that the growth behavior of β-$Ni(OH)_2$ nuclei into nanosheets is due to the intrinsic anisotropic characteristics of hexagonal crystal structure. The (001) plane of a hexagonal structure is a chemically active surface; therefore, rapid crystal growth along the [0001] direction is favorable [16-17]. Since the hydrothermal synthesis was performed without additional templates or additives, any differences in the size and morphology of the β-$Ni(OH)_2$ should be due to the anions used. Previous density functional theory (DFT) calculations [18] have reported that the hexagonal β-$Ni(OH)_2$ crystals had anisotropic Born effective charge tensor, indicating that the ionic configuration of Ni atom was located at the plane perpendicular to the *c*-axis. Moreover, as proved in the previously report [19], the negative charge of anions was selectively adsorbed on the (001) surface of the hexagonal β-$Ni(OH)_2$ crystals. The partial negative charges at the oxygen atom of the acetate (CH_3COO^-) and nitrate (NO_3^-) anions were evaluated via density functional theory DFT method with the B3LYP functional [20-21] and cc-pVQZ basis set [22] in GAUSSIAN03, are -0.640 and -0.471, respectively. The higher partial negative charge of the oxygen atom, the stronger the electrostatic interaction between an anion and the β-$Ni(OH)_2$ surface. Hence, the acetate anion suppressed the growth of the (001) surface of the crystals. This is the reason that the nanosheets of β-$Ni(OH)_2$ crystals prepared using acetate anions are shorter than those prepared using nitrate anions. Figure 3(c) is a higher-magnification TEM image of the β-$Ni(OH)_2$ nanosheets synthesized in the presence of nitrate anion and the inset of Figure 3(c) is the corresponding selected area electron diffraction (SAED) pattern. The diffraction spot can be interpreted as hexagonal $Ni(OH)_2$ crystals with an electron beam along the [001] direction. It indicates that the nanosheets are growing along the [001] direction of the crystal axis of the β-$Ni(OH)_2$. In addition, the high-resolution TEM (HRTEM) image (Figure 3(d)) clearly reveals (110) atomic planes with a spacing of 0.15 nm, confirming that the nanosheets are single crystals with a preferential [001] growth direction along their long axes. These results are consistent with the (001) preferred orientation revealed by the XRD results (Figure 1(a)).

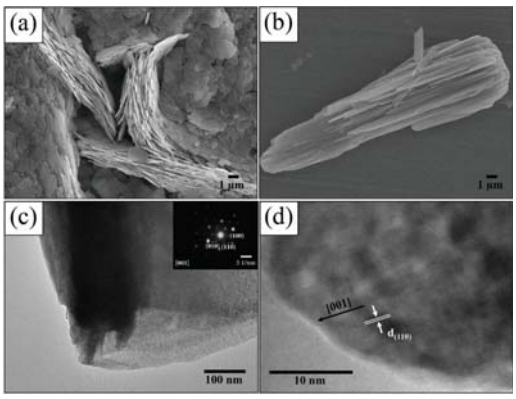

Figure 3. (a and b)FESEM images of the β-$Ni(OH)_2$ powders synthesized using different nickel salts, and (c) TEM and (d) HRTEM images of the β-$Ni(OH)_2$ powders synthesized using nickel nitrate. The inset of (c) is the corresponding SAED pattern.

After calcination, the morphology of the A500 and N500 NiO particles remained unchanged as shown in Figures4(a) and 4(b), respectively. The broken splinter-like shape(Figure 4(b)) may be due to the

ultrasonic treatment during FESEM sample preparation. Notably, the A500 and N500 NiO nanosheets contained many mesopores, as clearly observed in the TEM images shown in Figures 4(c) and 4(d), respectively. The diameters of the mesopores in the A500 NiO nanosheets (10-20 nm) are larger than thosein the N500 NiO nanosheets (6-10 nm). The surface areas of the A500 and N500 NiO particles are 33.21 and 88.11 m^2/g, respectively, using BET adsorption of nitrogen gas at the temperature of liquid nitrogen. The transformation of the β-$Ni(OH)_2$ into the NiO with a porous structure is accompanied by a volume contraction during dehydration/ thermal decomposition process and the intrinsic crystal contraction [23]. The corresponding SAED patterns of the A500 (Figure 4(e)) and N500 (Figure 4(f)) NiO nanosheets indicate that they consist of a single-crystalline structure. All diffraction spots can be interpreted as cubic NiO in accordance with the XRD results. Diffraction patterns of the A500 and N500 NiO particles with $[\bar{1}1\bar{1}]$ zone axis, simulated by CaRIne Crystallography 3.1 software, are shown in Figures 4(g) and 4(h). The a*, b* and c* reciprocal lattice vectors for both patterns are in the [100], [010], and [001] directions, respectively. The SAED and simulated diffraction patterns accord well. The single-crystalline nature of the NiO nanosheetsis a result of the conversion from β-$Ni(OH)_2$ to NiO. Although NiO is a face-centered cubic structure, the symmetry of the lattice array in the (111) plane is the same as that in the (001) plane of the hexagonal $Ni(OH)_2$ [7, 24]. Therefore, β-$Ni(OH)_2$ is a smooth transformation to NiO without destruction of the morphology, and the (001) plane in hexagonal crystal of β-$Ni(OH)_2$ becomes the (111) plane in the cubic crystal of NiO [24].

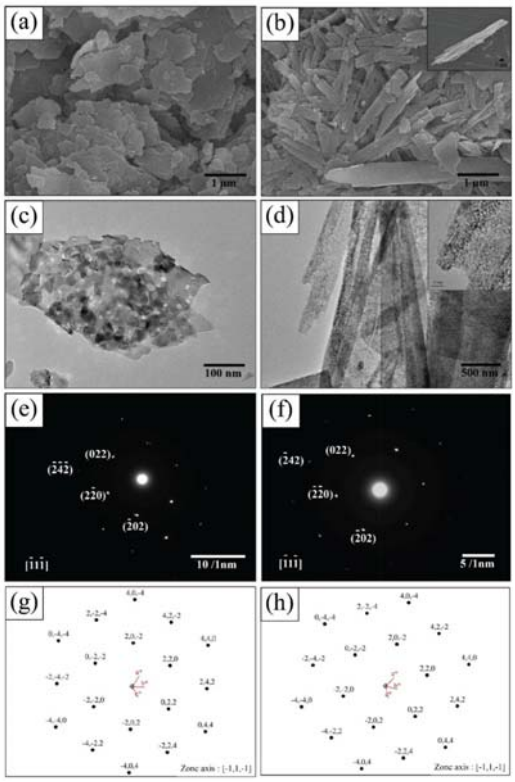

Figure 4. (a and b) FESEM images, (c and d) TEM images, (e and f) SAED patterns, and (g and h) simulated diffraction patterns of the NiO powders synthesized using different nickel salts. The inset of (b) shows the splinter-like structure of the N500 NiO powder and the inset of (d) is the corresponding higher magnified image.

EDX spectra of the NiO powders shown in Figure 5 demonstrate the existence of Ni and O elements, where the atomic ratios of Ni:O are close to the stoichiometry of NiO. Au and C elements came from the coated gold and environment, respectively. Figure 6 shows the UV-Vis absorption spectra of the NiO powders. The N500 NiO powder exhibits stronger light absorption compared to the A500 NiO powder. The stronger light absorption could be due to the increase in the optical path that captures the light more efficiently by scattering between

the porous long nanosheets of the N500 NiO powder. This result indicates that size, morphology, and surface area are the important factors affecting light absorption ability.

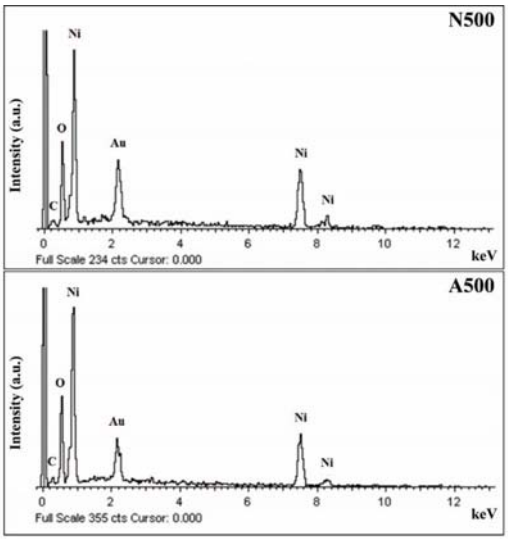

Figure 5. EDX spectra of the NiO powders.

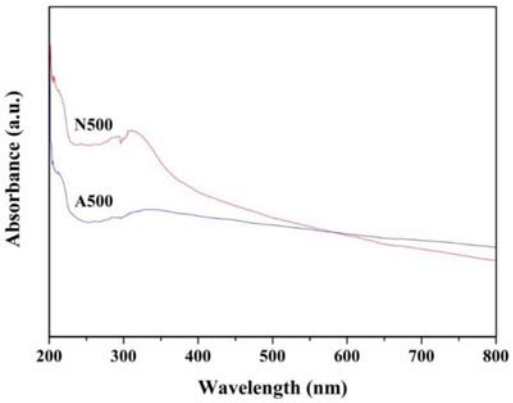

Figure 6. UV-Vis absorption spectra of the NiO powders.

4. CONCLUSION

Using different nickel sources as starting reagents for hydrothermal synthesis of NiO nanostructures firstly resulted in β-$Ni(OH)_2$ nanostructures with different architectures. The obtained β-$Ni(OH)_2$ nanostructures were then transformed via calcination to porous NiO nanostructures with unchanged morphology. The difference in the interaction ability between the anions and the β-$Ni(OH)_2$ surfaces affected the growth behavior of the nanocrystals.

ACKNOWLEDGEMENTS

This work was supported by the Chiang Mai University (CMU) Junior Research Fellowship Program and the National Research University (NRU) Project under Thailand's Office of the Higher Education Commission, Materials Science Research Center and Chiang Mai University. Pranwadee Kaewmuang would like to thank the Graduate School of Chiang Mai University.

REFERENCES

[1] Min J., Liu J., Lei M., Wang W., Lu Y., Yang L., Yang Q., Liu G. and Su N., *ACS Appl. Mater. Interf.*, 2016; **8**: 780-791. DOI 10.1021/acsami.5b09997.

[2] Tadic M., Nikolic D., Panjan M. and Blake G.R., *J. Alloys Compd.*, 2015; **647**: 1061-1068. DOI 10.1016/j.jallcom.2015.06.027.

[3] Nattestad A., Ferguson M., Kerr R., Cheng Y.B. and Bach U., *Nanotechnology*, 2008; **19**: 295304-295312. DOI 10.1088/0957-4484/19/29/295304.

[4] San X., Wang G., Liang B., Ma J., Meng D. and Shen Y., *J. Alloys Compd.*, 2015; **636**:357-362. DOI 10.1016/j.jallcom.2015.02.191.

[5] Dong Q., Yin S., Guo C., Wu X., Kumada N., Takei T., Miura A., Yonesaki Y. and Sato T., *Appl. Catal. B: Environ.*, 2014; **147**: 741-747. DOI 10.1016/j.apcatb.2013.10.007.

[6] Qiu Y., Yu J., Tan C. and Yin J., *Mater. Lett.*, 2009; **63**: 200-202. DOI 10.1016/j.matlet.2008.09.030.

[7] Li Y., Tan B. and Wu Y., *Chem. Mater.*, 2008; **20**: 567-576. DOI 10.1021/cm 070784g.

[8] Beach E., Brown S., Shqau K., Mottern M., Warchol Z. and Morris P., *Mater. Lett.*, 2008; **62**: 1957-1960. DOI 10.1016/j. matlet.2007.10.050.

[9] Christy A.J. and Umadevi M., *Mater. Res. Bull.*, 2013; **48**: 4248-4254. DOI 10.1016/j.materresbull.2013.06.072.

[10] Zhong J., Wang X.L., Xia X.H., Gu C.D., Xiang J.Y., Zhang J. and Tu J.P., *J. Alloys Compd.*, 2011; **509**: 3889-3893. DOI 10.1016/j.jallcom.2010.12.151.

[11] Sun D., Zhang J., Ren H., Cui Z. and Sun D., *J. Phys. Chem. C*, 2010; **114**: 12110-12116. DOI 10.1021/jp1033849.

[12] Zhu W., Shui A., Xu L., Cheng X., Liu P. and Wang H., *Ultrason. Sonochem.*, 2014; **21**: 1707-1713. DOI 10.1016/j.ultsonch. 2014.02.026.

[13] Khan Y., Durrani S.K., Mehmood M., Jan A. and Abbasi M.A., *Mater. Chem. Phys.*, 2011; **130**: 1169-1174. DOI 10.1016/j.matchemphys.2011.08.052.

[14] Freitas M.B.J.G., *J. Power Sources*, 2001; **93**: 163-173. DOI 10.1016/S0378-7753 (00)00570-X.

[15] Al-Hajry A., Umar A., Vaseem M., Al-Assiri M.S., El-Tantawy F., Bououdina M., Al-Heniti S. and Hahn Y.B., *Superlattice Microst.*, 2008; **44**: 216-222. DOI 10.1016/j.spmi.2008.04.008.

[16] Li W., Shi E., Zhong W. and Yin Z., *J. Cryst. Growth*, 1999; **203**: 186-196. DOI 10.1016/S0022-0248(99)00076-7.

[17] Abbasi M.A., Khan Y., Hussain S., Nur O. and Willander M., *Vacuum*, 2012; **86**: 1998-2001. DOI 10.1016/j. vacuum.2012.05.020.

[18] Hermet P., Gourrier L., Bantignies J.L., Ravot D., Michel T., Deabate S., Boulet P. and Henn F., *Phys. Rev. B*, 2011; **84**: 235-211. DOI 10.1103/PhysRevB.84. 235211.

[19] Dong L., Chu Y. and Sun W., *Chem. Eur. J.*, 2008; **14**: 5064-5072. DOI 10.1002/ chem.200701627.

[20] Lee C., Yang W. and Parr R.G., *Phys. Rev. B*, 1988; **37**: 785-789. DOI 10.1103/ PhysRevB.37.785.

[21] Becke A.D., *J. Chem. Phys.*, 1993; **98**: 5648-5652. DOI 10.1063/1.464913.

[22] Woon D.E. and Dunning Jr.T.H., *J. Chem. Phys.*, 1993; **98**: 1358-1371. DOI 10.1063/1.464303.

[23] Sharma R.K. and Ghose R., *Superlattice Microst.*, 2015; **80**: 169-180. DOI 10.1016/j.spmi.2014.12.034.

[24] Kuang D., Lei B., Pan Y., Yu X. and Su C., *J. Phys. Chem. C*, 2009; **113**: 5508-5513. DOI 10.1021/jp809013g.